Available online at www.sciencedirect.com
ScienceDirect
Journal of Power Sources 160 (2006) 413–421
JOURNAL OF POWER SOURCES
www.elsevier.com/locate/jpowsour

A three-dimensional mathematical model for liquid-fed direct methanol fuel cells

Jiabin Ge, Hongtan Liu *

Department of Mechanical and Aerospace Engineering, University of Miami, Coral Gables, FL 33124, USA

Received 9 December 2005; received in revised form 31 January 2006; accepted 1 February 2006
Available online 9 March 2006

Abstract

A three-dimensional, single-phase, multi-component mathematical model has been developed for a liquid-fed direct methanol fuel cell (DMFC). The traditional continuity, momentum, and species conservation equations are coupled with electrochemical kinetics in both the anode and cathode catalyst layer. At the anode side, the liquid phase is considered, and at the cathode side only the gas phase is considered. Methanol crossover due to both diffusion and electro-osmotic drag from the anode to the cathode is taken into consideration and the effect is incorporated into the model using a mixed-potential at the cathode. A finite-volume-based CFD technique is used to develop the in-house numerical code and the code is successfully used to simulate the fuel cell performance as well as the multi-component behavior in a DMFC. The modeling results of polarization curves compare well with our experimental data. Subsequently, the model is used to study the effects of methanol crossover, the effects of porosities of the diffusion layer and the catalyst layer, the effects of methanol flow rates, and the effects of the channel shoulder widths.

Keywords: DMFC; Mathematical model

1. Introduction

The direct methanol fuel cell (DMFC) is considered a highly promising power source with its important attributes of quick refueling, low temperature and pressure, low methanol cost, no liquid electrolyte, and compact cell design, etc. Efforts in developing mathematical models for DMFCs have been limited until recent years. Baxter et al. [1] developed a one-dimensional and single-phase mathematical model for a liquid-fed DMFC, focusing on the anode catalyst layer. Dhole et al. [2] presented a one-dimensional model for the vapor-fed DMFC and the crossover effects were studied. Scott et al. [3,4] developed several simplified single-phase models to study transport and electrochemical processes in a liquid-fed DMFC and showed that the cell performance is limited by the slow diffusion of methanol in liquid. Scott and co-workers [5] also developed a model to predict the effective methanol concentration at the catalyst surface. This model, together with an empirical model of the open circuit voltage and the cathode over-potential model, was used to predict the overall cell voltage and current density. Cruickshank and Scott [6] presented a simple model to describe methanol permeation. Shukla et al. [7] developed a one-dimensional model to compare the performance of a solid-polymer electrolyte DMFC with aqueous methanol and methanol mixed with air at the anode side. Kulikovsky et al. [8] simulated a vapor-fed DMFC with a two-dimensional model and compared the detailed current density distributions in the backing, catalyst layer, and membrane separator between a conventional and a new current collector. Wang and Wang [9] developed two-dimensional, two-phase and multi-component model for a liquid-fed DMFC. In this model, they considered the mixed potential effects of methanol oxidation due to methanol crossover, but the catalyst layers were treated as infinitely thin interfaces. Birgersson et al. [10] developed a two-dimensional and single-phase model for the anode of a DMFC. In their model, the catalyst layer was taken into consideration as boundary conditions via parameter adaptation. Divisek et al. [11] accounted for the influence of both the methanol and oxygen reaction kinetics and their dependency on the two-phase mass flow in the catalyst and diffusion layers by a vapor–liquid model for the DMFC. In this work, we have developed a three-dimensional, single-phase and multi-component model for the entire DMFC, including both the anode and cathode channels,

* Corresponding author. Tel.: +1 3052842019; fax: +1 3052842580.
E-mail address: hliu@miami.edu (H. Liu).

0378-7753/$ – see front matter © 2006 Elsevier B.V. All rights reserved.
doi:10.1016/j.jpowsour.2006.02.001

Nomenclature

a	water activity
ai_a^{ref}	reference exchange current density times specific area at anode ($A\,m^{-3}$)
ai_c^{ref}	reference exchange current density time specific area at cathode ($A\,m^{-3}$)
C	molar concentration ($mol\,m^{-3}$)
D	diffusion coefficient ($m^2\,s^{-1}$)
E	voltage (V)
F	Faraday's constant ($C\,mol^{-1}$)
h_c	channel depth (z direction width) (m)
I	current density ($A\,m^{-2}$)
j	transfer current density ($A\,m^{-3}$)
k_ϕ	electrokinetic permeability of membrane (m^2)
k_h	hydraulic permeability (m^2)
k_{air}	permeability to air of gas diffuser (m^2)
k_w	permeability to water of gas diffuser (m^2)
L_c	channel length (y direction width) (m)
M	molecular weight ($g\,mol^{-1}$)
N	mole flux ($mol\,m^{-2}\,s^{-1}$)
P	pressure ($N\,m^{-3}$)
Q	flow rate ($m^3\,s^{-1}$)
r_ε	porous media correction factor
R	resistance (Ω)
R_c	gas constant ($J\,mol^{-1}\,K^{-1}$)
S	source term
t_d	diffusion layer thickness (m)
t_c	catalyst layer thickness (m)
t_m	membrane thickness (m)
T	temperature (K)
V	velocity ($m\,s^{-1}$)
w_c	half-channel width (m)
w_s	collector plate width (m)
X	mole fraction
z	charge of fixed (sulfonate) sites

Greek symbols

α	transfer coefficient
ε	porosity
γ	reaction order
λ	electro-osmotic drag coefficient
μ	viscosity ($kg\,m^{-1}\,s^{-1}$)
ρ	density ($kg\,m^{-3}$)
σ	conductivity ($1/(\Omega\,m)$)
ψ	water content in the membrane

Subscripts and superscripts

a	anode, air
c	cathode
ca	catalyst layer
cross	methanol crossover
CH	methanol
d	diffusion
eff	effective
g	gas
H^+	proton
i	ith layer
k	kth component
l	liquid water
m	membrane
O	oxygen
ref	reference
w	water

both diffusion layers, and both catalyst layers and the membrane. The model for the anode and cathode sides is coupled by current density. The modeling results of polarization curves compared well with our experimental data and this model is used to study the effects of methanol crossover and various parameter effects.

2. Mathematical model

2.1. Model description

The modeling domain for the DMFC consists of the anode side, the cathode side, and the membrane as shown in Fig. 1. Both the anode and cathode sides have the same structure and can be sub-divided into the gas channel, the diffusion layer, and the catalyst layer. In Fig. 1, h_c is the gas channel height; t_d, t_c, t_m the thickness of the diffusion layer, the catalyst layer, and the membrane, respectively; w_c, w_s, w_t are the half-widths of the gas channel, the collector plate, and the diffusion layer, respectively; and L_c is the length along the channel. The reactants enter the gas channels from the surface at $y=0$. The detailed geometric parameters are given in Table 1.

Two components, methanol and water, were considered at the anode side, and air was considered at the cathode side.

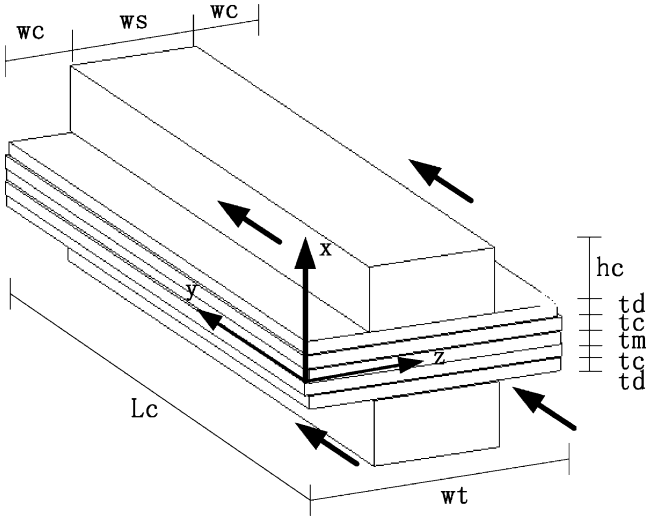

Fig. 1. Schematic of the modeling domain.

Table 1
Geometric parameters used in the model

Channel length (L_c)	6.5×10^{-2} m
Half-channel width (w_c)	5.0×10^{-4} m
Channel height (h_c)	8×10^{-4} m
Channel shoulder width (w_s)	1.0×10^{-3} m
Diffusion layer thickness (t_d)	1.4×10^{-4} m
Catalyst layer thickness (t_c)	3×10^{-5} m
Membrane thickness (Nafion® 117) (t_m)	1.8×10^{-4} m

Table 2
r_ε and S_i in momentum equations

	r_ε	S_i
Channel	1.0	0
Diffuser	$2.25\left(\frac{1}{\varepsilon_d} - 1\right)^2$	$-\varepsilon_d \frac{\mu}{k} \vec{V}$
Catalyst	$2.25\left(\frac{1}{\varepsilon_c} - 1\right)^2$	$-\varepsilon_c \frac{\mu}{k} \vec{V} + \frac{k_\phi}{k_h} c_{H^+} z F \nabla\phi$

2.2. Model assumptions

In the model development, the following assumptions are used: fluids are incompressible; all the flows are laminar and all the processes are steady state as well as isothermal; the effects of carbon dioxide generated in the anode side are negligible; methanol crossed over from the anode to the cathode is completely oxidized at the interface between the membrane and the cathode catalyst layer; and the membrane is impermeable to gases and is fully hydrated.

Table 3
Anode and cathode source term (s_k) in species equations

	Anode (source term s_k)			Cathode (source term s_k)		
	Methanol	Water	Proton	Oxygen	Water	Proton
Channel layers	0	0	0	0	0	0
Diffusion layers	0	0	0	0	0	0
Catalyst layers	$-\frac{M_m}{6F} j_a$	$-\frac{M_w}{6F} j_a$	$\frac{1}{F} j_a$	$\frac{M_O}{4F} j_c$	$-\frac{M_w}{2F} j_c$	$\frac{1}{F} j_c$

2.3. Model equations

On both the anode and cathode sides, the governing equations for the flow field and species concentration are in the same form. The appropriate model equations in vector forms are listed below.

Continuity equation

$$\nabla \cdot \vec{V} = 0 \tag{1}$$

Momentum equation

$$\rho \vec{V} \cdot \nabla \vec{V} = -\nabla P + r_\varepsilon \mu \nabla^2 \vec{V} + \rho S_i \tag{2}$$

In the momentum equations and Table 2, ε_d and ε_c are the porosities of the diffusion layer and catalyst layer, respectively, r_ε the porous media correction factor, k the permeability of water (k_w) in the anode and the permeability of air (k_{air}) in the cathode, k_ϕ the electrokinetic permeability of the membrane, k_h the hydraulic permeability of the membrane, z the charge number of

Table 4
Physical parameters and basic operation conditions

Cell temperature	$T = 343$ K	
Pressure	$P = 1.013 \times 10^5$ N m^{-2}	
Anode reactant flow rate	$Q_a^{inlet} = 10^{-5}$ m^3 s^{-1}	
Cathode reactant flow rate	$Q_c^{inlet} = 2 \times 10^{-5}$ m^3 s^{-1}	
Inlet oxygen mole fraction	$X_O^{inlet} = 0.21$	
Inlet methanol concentration	$C_{CH}^{inlet} = 1000$ mol m^{-3}	
Methanol reference concentration	$C_{CH}^{ref} = 2000$ mol m^{-3}	
Oxygen reference concentration	$C_O^{ref} = 0.472$ mol m^{-3}	[7]
Diffusion coefficient of oxygen in air	$D_O = 1.22 \times 10^{-10}$ m^2 s^{-1}	
Diffusion coefficient of methanol in water	$D_{CH} = 2.8 \times 10^{-9}$ m^2 s^{-1}	[4]
Porosity of diffusion layer	$\varepsilon_d = 0.6$	
Porosity of catalyst layer	$\varepsilon_c = 0.4$	
Porosity of membrane	$\varepsilon_m = 0.28$	[16]
Permeability to air in the gas diffuser	$k_{air} = 1.76 \times 10^{-11}$ m^2	
Permeability to water in the gas diffuser	$k_w = 1.0 \times 10^{-11}$ m^2	
Air density	$\rho_{air} = 1.0$ kg m^{-3}	
Water density	$\rho_w = 1000$ kg m^{-3}	
Air viscosity	$\mu_g = 2.05 \times 10^{-5}$ kg m^{-1} s^{-1}	
Electrokinetic permeability of the membrane	$k_\phi = 7.18 \times 10^{-20}$ m^2	[16]
Hydraulic permeability of the membrane	$k_p = 1.8 \times 10^{-18}$ m^2	[16]
Gas constant	$R_c = 8.314$ J mol^{-1} K^{-1}	
Reference exchange current density times specific area at anode	$ai_a^{ref} = 1.0 \times 10^6$ A m^{-3}	[4]
Reference exchange current density times specific area at cathode	$ai_c^{ref} = 200$ A m^{-3}	[7]
Anode reaction order	$\gamma_a = 1.0$	[7]
Cathode reaction order	$\gamma_c = 1.0$	[7]
Electro-osmotic drag coefficient of water	$\lambda_w = 2.5$	[1]
Anode transfer coefficient	$\alpha_a = 0.5$	[7]
Cathode transfer coefficient	$\alpha_c = 0.5$	
Charge of fixed (sulfonate) sites	$z = -1$	

the fixed sites, c_{H^+} the concentration of protons that is taken to be the concentration of the fixed charge and ϕ is the membrane phase potential.

Species equations

$$\rho\vec{V}\cdot\nabla X_k = \rho D_k^{\text{eff}}\nabla^2 X_k + S_k \tag{3}$$

$$\sum_k X_k = 1 \tag{4}$$

In Eqs. (3) and (4) as well as Table 3, k represents methanol or water in the anode side, and oxygen, nitrogen, or water vapor in the cathode side, X_k the mole fraction of species k, S_k the mass generation rate for species k per unit volume, D_k^{eff} the effective diffusion coefficient of the kth component and j_a and j_c are the volumetric current density of anode and cathode, respectively. The effective diffusivity is given by:

$$D_k^{\text{eff}} = D_k\varepsilon^{1.5} \tag{5}$$

where ε is the porosity of porous media and D_k is the diffusivity of the kth component.

2.3.1. Electrochemical kinetics in catalyst layers

The Tafel equation is used to determine the transfer current densities j_c and j_a:

$$j_a = \text{ai}_a^{\text{ref}}\left(\frac{X_{CH}}{X_{CH}^{\text{ref}}}\right)^{\gamma_a}\exp\left(\frac{\alpha_a F}{R_c T}\eta_a\right) \tag{6}$$

$$j_c = -\text{ai}_c^{\text{ref}}\left(\frac{X_O}{X_O^{\text{ref}}}\right)^{\gamma_c}\exp\left(-\frac{\alpha_c F}{R_c T}\eta_c\right) \tag{7}$$

where ai_a^{ref} and ai_c^{ref} are the reference exchange currents density multiplied by the specific area at the anode and cathode sides, respectively, γ_a and γ_c the anode and cathode reaction order, η_a and η_c the anode and cathode over-potential and α_a and α_c are the anode and cathode transfer coefficients, respectively.

2.3.2. Cell potential and current density

The cell voltage is calculated by:

$$E_{\text{cell}} = E_0 - \eta_a + \eta_c - IR_m \tag{8}$$

where E_0 is the open circuit voltage, R_m the membrane resistance and I is the average current density of the cell and is given by:

$$I = \int_0^{t_c} j_a\,\mathrm{d}z \tag{9}$$

where t_c is the catalyst layer thickness.

The membrane is in direct contact with liquid water at the anode side and water is produced at the cathode side. Besides, water is also supplied to the cathode side by electro-osmosis. Thus, it is a reasonably to assume the membrane is always fully hydrated and for a fully hydrated membrane its ionic conductivity can be determined by [12]:

$$\sigma_m(T) = \sigma_m^{\text{ref}}\exp\left[1268\left(\frac{1}{303}-\frac{1}{T}\right)\right] \tag{10}$$

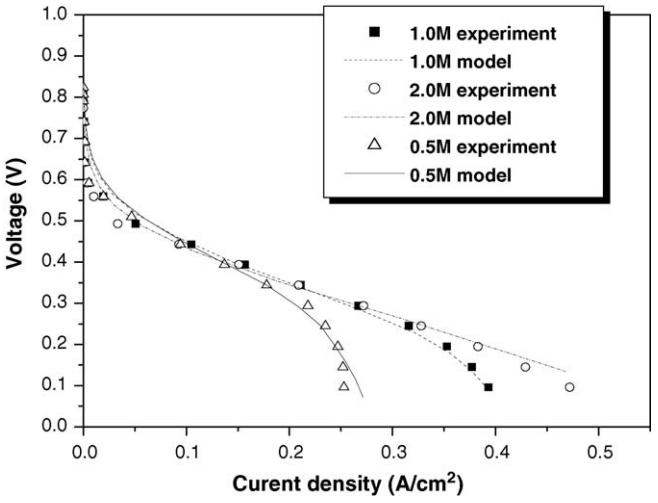

Fig. 2. Comparison of modeling results with experimental data at different methanol feed concentrations. The cell temperature 70 °C, cathode humidification temperature 70 °C, methanol flow rate 6 ml min^{-1}, and air flow rate 1200 sccm.

where σ_m^{ref} is the reference ionic conductivity at 303 K.

The resistance of the membrane is defined by:

$$R_m = \int_0^{t_m}\frac{1}{\sigma_m}\,\mathrm{d}z = \frac{t_m}{\sigma_m} \tag{11}$$

where t_m is the thickness of the membrane and σ_m is the membrane conductivity.

2.3.3. Methanol crossover

The methanol transport is treated similarly to the water transport. In the membrane, the methanol transfer is caused by diffusion and electro-osmotic drag, and the methanol flux is given by [4]:

$$N_{CH}^m = \frac{\lambda_{CH} I}{F} - \varepsilon_m^{1.5} D_{CH}^m\frac{\mathrm{d}C_{CH}^m}{\mathrm{d}z} \tag{12}$$

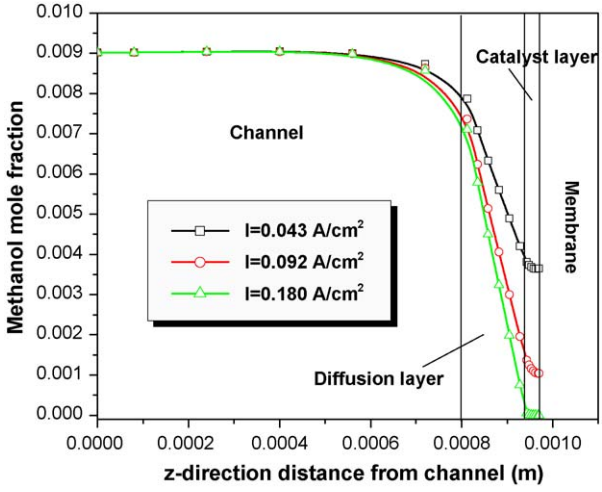

Fig. 3. Average methanol mole fraction profiles at different current densities. The cell temperature 70 °C, methanol feed concentration 0.5 M, methanol flow rate 6 ml min^{-1}, and air flow rate 1200 sccm.

where C^{m}_{CH} is the methanol concentration in the membrane. The electro-osmotic drag coefficient for methanol, λ_{CH}, is defined as the number of methanol molecules dragged by each proton through the membrane, (CH_3OH/H^+), and it is given by [13]:

$$\lambda_{CH} = X_{CH}|_{ac/m}\lambda_w \quad (13)$$

where $X_{CH}|_{ac/m}$ is the methanol mole fraction at the interface between the anode catalyst layer and the membrane.

The diffusion coefficient of methanol in the membrane (D^{m}_{CH}) is given by [4]:

$$D^{m}_{CH} = 4.012 \times 10^{-13} \exp(0.024312T)\,(m^2\,s^{-1}) \quad (14)$$

2.4. Solution method

The velocity fields at the anode and cathode sides are determined first. For a given value of the anode over-potential η_a, the species concentration and the average current density at the anode side are determined. Then the flux of methanol crossover can be calculated and the pseudo current density due to methanol crossover is determined by:

$$I_{cross} = \frac{N^{m}_{CH}}{6F} \quad (15)$$

Using species equations and the Tafel equation in the cathode side iteratively [9]:

$$(I + I_{cross})\frac{1}{t_c} = -ai^{ref}_{c}\left(\frac{X_O}{X^{ref}_O}\right)^{\gamma_c} \exp\left(-\frac{\alpha_c F}{R_c T}\eta_c\right) \quad (16)$$

the cathode over-potential can be determined and the cell voltage is calculated using Eq. (8). Then another value of η_a is given and the process is repeated until the entire polarization curve is obtained.

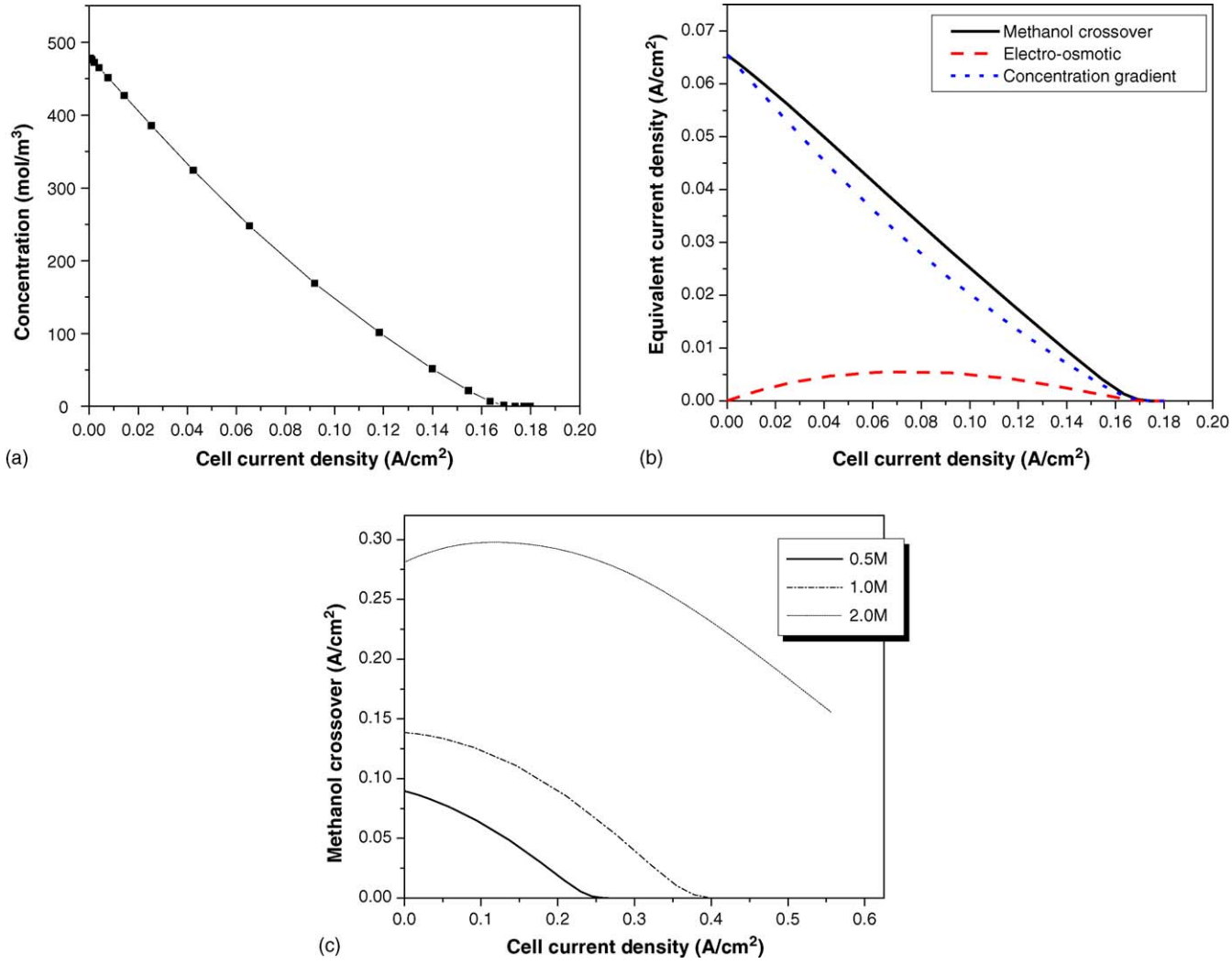

Fig. 4. (a) Methanol concentration vs. cell current density at the anode/membrane interface. The cell temperature is 70 °C, methanol flow rate 6 ml min^{-1} and air flow rate 1200 sccm. (b) Equivalent current density vs. cell current density. The cell temperature 70 °C, methanol flow rate 6 ml min^{-1} and air flow rate 1200 sccm. (c) Equivalent current density of methanol crossover vs. cell current density at different methanol concentrations. The cell temperature 70 °C, methanol flow rate 6 ml min^{-1}, and air flow rate 1200 sccm.

3. Modeling results and discussions

3.1. Comparison with experimental data

The geometric parameters used in the model are the same as those used in our previous experimental studies [14] and are listed in Table 1. The physical parameters and basic operating conditions are tabulated in Table 4. Typical modeling results of cell polarization curves at different methanol concentrations are shown in Fig. 2 and compared with the experimental results [14]. The cell temperature is 70 °C, cathode humidification temperature is 70 °C, methanol flow rate is 6 ml min^{-1}, and air flow rate is 1200 sccm. It is seen from Fig. 2 that the three-dimensional modeling results show good agreement with the experimental data.

Fig. 3 shows average methanol fraction profiles at three different cell current densities. The modeling result suggests that the gas diffusion layer contributes a substantial fraction of the total mass transfer resistance, which indicates the need of work and improvement in the gas diffusion layer. This result is in agreement with those obtained by Scott et al. [3,4] that the cell performance is limited by the slow diffusion of methanol in liquid water.

3.2. Effect of methanol crossover

Fig. 4(a) shows the methanol concentration contribution at different current densities on the interface between the anode catalyst layer and the membrane. Fig. 4(b) shows the cell current density versus the equivalent crossover current densities, which includes both the electro-osmotic drag flux and the diffusion flux. Fig. 4(c) shows the modeling results of equivalent crossover current densities at different cell current densities.

Generally speaking, the amount of methanol crossover decreases with current density, and this trend is in good agreement with those reported in the literatures [2,15]. As mentioned earlier, methanol crossover is mainly due to the diffusion and the electro-osmosis. The diffusion flux is proportional to the methanol concentration gradient across the membrane. At the interface between the anode catalyst layer and the membrane methanol concentration decreases with current density. Thus it is easy to understand that the diffusive methanol flux decreases with current density. As shown in Eqs. (12) and (13), the methanol crossover flux due to electro-osmosis is proportional to both the current density and the methanol concentration at this interface since the methanol concentration is assumed to be zero at the membrane interface with the cathode catalyst layer. Therefore, lower concentration of methanol at this interface may also leads to lower electro-osmosis flux. As the current density increases to such a value that the methanol is depleted in the anode catalyst layer, the methanol crossover rate becomes zero. The zero diffusion flux is self-evident since the concentration gradient is zero. When the methanol concentration at the interface between the anode catalyst layer and the membrane becomes zero, no matter how much water is transferred due to electro-osmosis, no methanol is present in water, thus methanol transfer due to electro-osmosis is also zero.

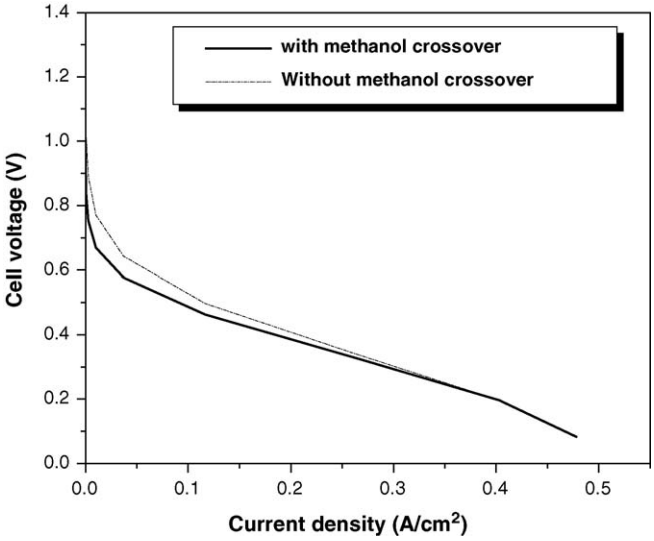

Fig. 5. Modeling results of the effect of methanol crossover with air flow on cell performance. The cell temperature is 70 °C, methanol concentration 1 M, methanol flow rate 6 ml min^{-1}, and oxygen flow rate 1200 sccm.

In Fig. 5, the polarization curve for a fuel cell without the effects of methanol crossover is compared with that with the effect of methanol crossover. It is clearly seen that, even at a very low methanol concentration, e.g. 1 M, the effect of methanol crossover is still significant.

3.3. Effect of porosities of diffusion layer and catalyst layer

Figs. 6–9 show the effects of porosities of the diffusion layer and the catalyst layer on the cell performance and methanol crossover. The cell temperature is 70 °C, methanol concentration is 0.5 M, methanol flow rate is 6 ml min^{-1} and air flow rate is 1200 sccm. From these results, it can be seen that the porosities of both the diffusion layer and the catalyst layer have significant

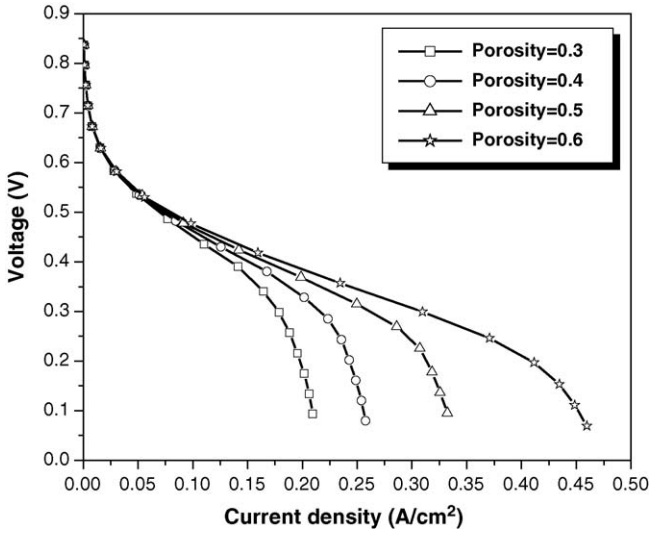

Fig. 6. Modeling results of the effect of porosity of catalyst layer on performance. The cell temperature is 70 °C, methanol concentration 0.5 M, methanol flow rate 6 ml min^{-1}, and air flow rate 1200 sccm.

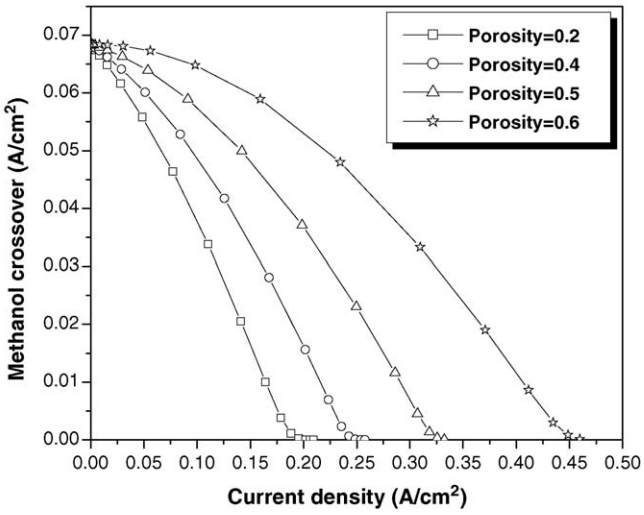

Fig. 7. Modeling results of the effect of porosity of catalyst layers on methanol crossover. The cell temperature is 70 °C, methanol concentration 0.5 M, methanol flow rate 6 ml min^{-1}, and air flow rate 1200 sccm.

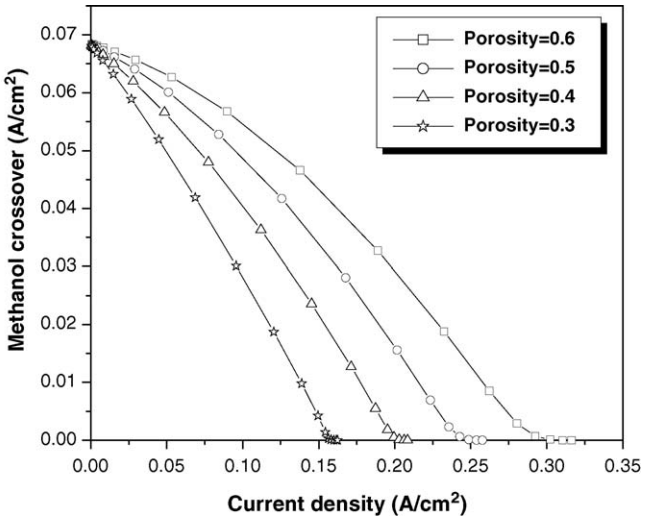

Fig. 9. Modeling results of the effect of porosity of diffusion layers on methanol crossover. The cell temperature is 70 °C, methanol concentration 0.5 M, methanol flow rate 6 ml min^{-1}, and air flow rate 1200 sccm.

effects on cell performances. The performance and methanol crossover increase with the porosity. These results again indicate that the slow diffusion of methanol in liquid water is a liming factor in DMFC performances.

Fig. 6 shows the effects of porosity of the anode catalyst layer on the cell performances. The modeling suggests that the catalyst layer porosity has a significant influence on the cell performance. Fig. 7 shows the effects of porosity of the anode catalyst layer on methanol crossover. Fig. 8 shows the effects of porosity of the anode diffusion layers on the cell performances. Fig. 9 shows the effects of porosity of the anode diffusion layer on methanol crossover. Generally speaking, methanol crossover decreases with decrease in porosity in the anode diffusion layer; while the cell performance increases with the increase in porosity in both the anode diffusion layer and catalyst layer.

3.4. Effect of the methanol flow rate

Fig. 10 shows the polarization curves at different methanol flow rates. The cell temperature is 70 °C, methanol concentration is 0.5 M, and air flow rate is 1200 sccm. The current density increases with the anode methanol flow rate at the methanol concentration of 0.5 M. When the anode flow rate is higher than 7 ml min^{-1}, the cell current density does not change significantly with the anode flow rate. At low flow rate, due to mass transfer resistance, the methanol concentration is too low in the catalyst layer and causes a lower current density, especially at the down stream. When the flow rate is high enough, any further increase in the flow rate has no significant effect on the methanol concentration in the channel and in the catalyst layer, thus no significant effect on cell current density.

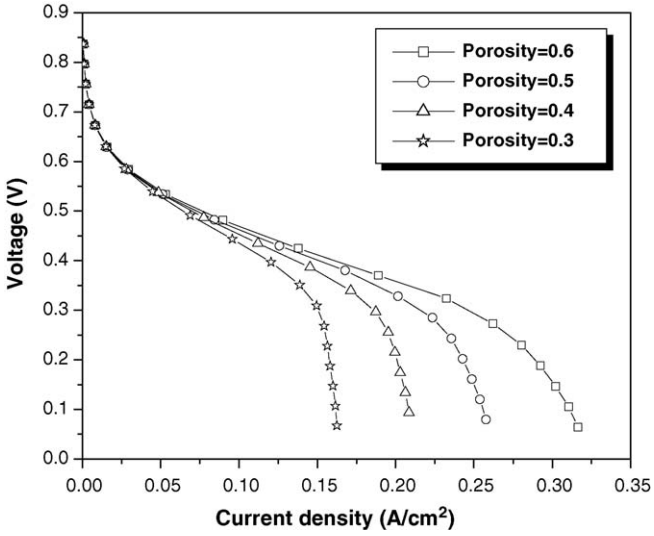

Fig. 8. Modeling results of the effect of porosity of diffusion layers on methanol crossover. The cell temperature is 70 °C, methanol concentration 0.5 M, methanol flow rate 6 ml min^{-1}, and air flow rate 1200 sccm.

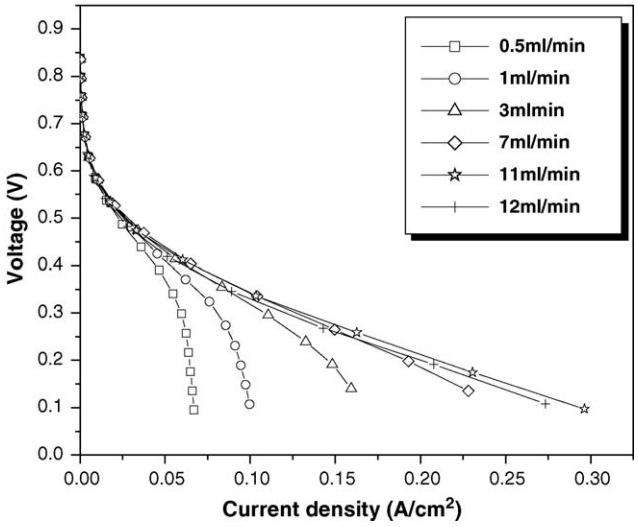

Fig. 10. Modeling results of polarization curves of different methanol feed flux. The cell temperature is 70 °C, methanol concentration 0.5 M, and air flow rate 1200 sccm.

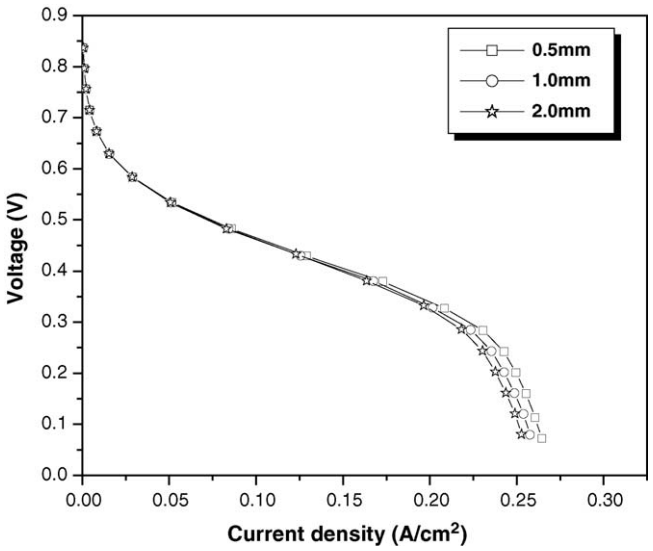

Fig. 11. Modeling results of the effect of channel shoulder width on performance. The cell temperature is 70 °C, methanol concentration 0.5 M, methanol flow rate 6 ml min^{-1}, and air flow rate 1200 sccm.

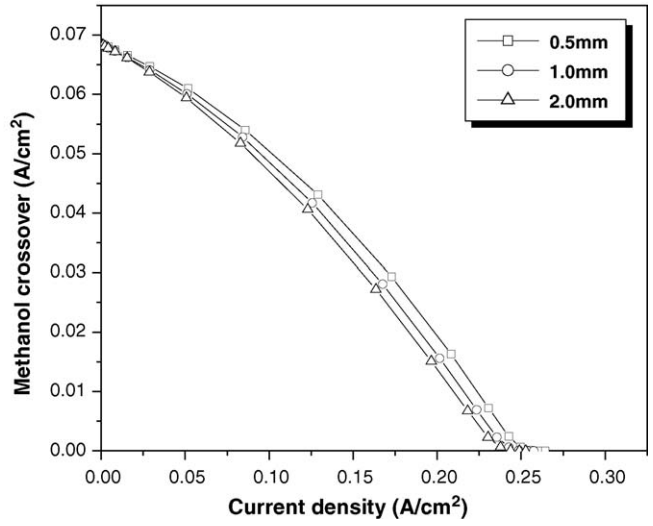

Fig. 12. Modeling results of the effect of channel shoulder width on methanol crossover. The cell temperature is 70 °C, methanol concentration 0.5 M, methanol flow rate 6 ml min^{-1}, and air flow rate 1200 sccm.

3.5. Effect of the channel shoulder width

Fig. 11 shows the effect of the channel shoulder width on the cell performance. It can be seen that the cell performance decreases with the channel shoulder width, but the effects are not significant. Fig. 12 shows the effect of the channel shoulder width on methanol crossover. The crossover decreases with the increase in shoulder width due to the blockage effect of the shoulders.

4. Concluding remarks

A three-dimensional, single-phase, multi-component model was developed for a liquid-fed direct methanol fuel cell (DMFC). The electrochemical kinetics in both the cathode and anode were coupled with the traditional continuity, momentum, and species conservation equations, and the effect of methanol crossover was also incorporated in the model using a mixed-potential at the cathode. A finite-volume-based CFD technique was used to develop the in-house numerical code and the code was successfully used to simulate the fuel cell performance and the multi-component behavior in a DMFC. The model was able to predict polarization curves at various different operating conditions and it was used to study the effects of methanol crossover, the effects of porosities of diffusion layers and catalyst layers, the effects of methanol flow rates, and the effects of the channel shoulder widths. The simulation results showed that the effect of methanol crossover is significant, even at a very low methanol concentrations; the methanol crossover flux, thus the effect on cell performance, decrease with increasing current density; both the porosities of the anode catalyst layer and the diffusion layer have significant effect on methanol crossover and the cell performance; the effect of flow field shoulder width is not significant.

It is known that both gas and liquid phases exist in the anode and cathode in a real DMFC and an accurate model needs to take such two-phase phenomena into consideration. Development of such a multi-dimensional and multi-phase flow model is underway.

References

[1] S.F. Baxter, V.S. Battaglia, R.E. White, Methanol fuel cell model: anode, J. Electrochem. Soc. 146 (2) (1999) 437–447.
[2] H. Dohle, H. Schmitz, T. Bewer, J. Mergel, D. Stolten, Development of a compact 500 W class direct methanol fuel cell stack, J. Power Sources 106 (2002) 313–322.
[3] P. Argyropoulos, K. Scott, W.M. Taama, Modeling pressure distribution and anode/cathode streams vapor–liquid equilibrium composition in liquid feed direct methanol fuel cells, Chem. Eng. J. V78 (2000) p29–p41.
[4] K. Scott, P. Argyropoulos, K. Sundmacher, A model for the liquid feed direct methanol fuel cell, J. Electroanal. Chem. V477 (1999) p97–p110.
[5] K. Sundmacher, K. Scott, Direct methanol polymer electrolyte fuel cell: analysis of charge and mass transfer in the vapor–liquid–solid system, Chem. Eng. Sci. V54 (1999) p2927–p2936.
[6] J. Cruickshank, K. Scott, The degree and effect of methanol crossover in direct methanol fuel cell, J. Power Sources 70 (1998) 40–47.
[7] A.K. Shukla, C.L. Jackson, K. Scott, G. Murgia, A solid-polymer electrolyte direct methanol fuel cell with a mixed reactant and air anode, J. Power Sources 111 (2002) 43–51.
[8] A.A. Kulikovsky, Two-dimensional numerical modeling of a direct methanol fuel cell, J. Appl. Electrochem. V30 (2000) p1005–p1014.
[9] Z.H. Wang, C.Y. Wang, Mathematical modeling of liquid-feed methanol fuel cells, J. Electrochem. Soc. 150 (4) (2003) A508–A519.
[10] E. Birgersson, J. Nordlund, H. Ekstrom, M. Vynnycky, G. Lindbergh, Reduced two-dimensional one-phase model for analysis of the anode of a DMFC, J. Electrochem. Soc. 150 (10) (2003) A1368–A1376.
[11] J. Divisek, J. Fuhrmann, K. Gartner, R. Jung, Performance modeling of a direct methanol fuel cell, J. Electrochem. Soc. 150 (6) (2003) A811–A825.
[12] T.E. Springer, T.A. Zawodzinski, S. Gottesfeld, Polymer electrolyte fuel cell model, J. Electrochem. Soc. 138 (8) (1991) 2334–2342.

[13] X. Ren, T.E. Springer, T.A. Zawodzingski, S. Gottesfeld, Methanol transport through Nafion membranes electro-osmotic drag effects on potential step measurements, J. Electrochem. Soc. 147 (2000) 466.
[14] J. Ge, H. Liu, Experimental studies of a direct methanol fuel cell, J. Power Sources 142 (2005) 56–69.
[15] K.T. Jeng, C.W. Chen, Modeling and simulation of a direct methanol fuel cell anode, J. Power Sources 112 (2002) 367–375.
[16] D.M. Bernardy, M.W. Verbrugge, Mathematical model of the solid-polymer-electrolyte fuel cell, J. Electrochem. Soc. V139 (1992).